Peaked Density Profiles in Low Collisionality H-modes in JET, ASDEX Upgrade and TCV

H. Weisen[1], C. Angioni[2], M. Maslov[1], A. Zabolotsky[1], M. Beurskens[3], C. Fuchs[2], L. Garzotti[4], C. Giroud[3], P. Mantica[6], D. Mazon[5], L. Porte[1], J. Stober[2], JET-EFDA contributors, the ASDEX Upgrade Team and the TCV Team

[1)]Ecole Polytechnique Fédérale de Lausanne, Centre de Recherches en Physique des Plasmas, Association EURATOM - Confédération Suisse, EPFL, 1015 Lausanne, Switzerland

[2)]Max Planck Institut für Plasmaphysik, IPP-Euratom Association, D-87748 Garching bei München, Germany

[3)] UKAEA-Fusion, United Kingdom Atomic Energy Authority, Abingdon, UK
[4)] Istituto Gas Ionisati, Assoziazione ENEA-CNR-Euratom, Padova, Italy
[5)] Association Euratom-CEA, CEA/DSM/DRFC CEA-Cadarache, France
[6)] Istituto di Fisica del Plasma, Assoziazione ENEA-CNR-Euratom, Milano, Italy

Abstract. Results from an extensive database analysis of JET and AUG density profiles in H-mode, show that the density peaking factor $n_{e0}/\langle n_e\rangle$ increases to above 1.5 as the effective collisionality drops to values close to those expected for ITER. On any single device density peaking is also strongly correlated with the Greenwald number N_G and the particle outward flux Γ from the neutral beam source, when applicable. Fully RF-heated H-modes in JET and TCV show that neutral beam fuelling is not the dominant contributor to density peaking. Multiple regression analyses are performed which show that in the combined database, collisionality is the most relevant parameter. Scalings for density peaking are proposed and implications for ITER performance are discussed.

1. Introduction

Peaked electron and fuel density profiles in reactor plasmas provide the advantage of higher reactivity, higher bootstrap fraction and stronger electron-ion coupling in the core, than obtained with flat density profiles at the same average density and stored energy. Several recent papers have established that the existence of peaked density profiles in tokamak discharges is neither due to the Ware pinch, nor to the particle source (be it by edge or neutral beam fuelling), although both of these processes may be minor contributors [Hoang, Zab2003, Weisen 2004 ,2006 Zab2005]. The cause for density peaking hence appears to be an anomalous pinch. While some of the observations are in qualitative agreement with some of the theoretical predictions [Baker, Weisen EPL, Angioni 2003, Zab 2003], it is fair to say that agreement of state-of-the-art gyrokinetic theory with observation has not yet been demonstrated [Angioni 2005, Estrada-Mila]. In these conditions, as for many other aspects in fusion research, the authors have resolved to an empirical approach, by combining evidence from different devices in order to obtain a scaling of the peaking factor and normalised density gradients that is suitable for extrapolation towards reactor conditions. Following separate investigations on AUG [Angioni 2003] and JET [Weisen 2005,2006] the data were combined into a single database, with the advantage of reduced colinearities in the regression variables

2. Combined JET-AUG Database

The dimensionless physics parameters ν_{eff}, β and ρ^*, are used here with the following definitions:

$$\rho^* = 0.3225(m_{eff}\langle T_e\rangle)^{1/2}/(aB_T)\ ;\ \nu_{eff} = 2\times10^{-14}\langle n_e\rangle R_0/\langle T_e\rangle^2\ ;\ \beta = 4.02\times10^{-3}\langle p\rangle/B_T^2\ .$$

The above definition of ν_{eff} omits the factor Z_{eff}, in effect assumed to be equal to 2. Geometrical plasma parameters like q_{95} and the edge triangularity δ are also considered. The geometrical major radius R_0, despite being dimensional, is also included in part of the analysis as a device label, in order to check its significance in the regressions.
Detailed edge source calculations [Zab 2005] have shown that the edge source cannot account for peaking. These findings were confirmed in experiments in He plasmas, which have the same peaking as deuterium with otherwise similar operational parameters, despite quenching of charge exchange chains due to the low cross sections for double charge exchange [Zab 2005]. Consequently, only fuelling by beams is considered. The beam heating and particle source profiles have been computed for all the observations by the PENCIL code for JET and the FAFNER code for AUG data. By casting the general diffusive law for the net particle flux Γ in steady state determined by the source in the form $\frac{\nabla n}{n} = -\frac{1}{D}(\frac{\Gamma}{n} + V)$, the NBI source contribution to the density peaking can be quantified by a dimensionless source term $\Gamma^* = \frac{R\Gamma}{nD} \cong 2T \frac{\chi}{D} \frac{\Gamma}{Q_{NBI}} \frac{Q_{NBI}}{Q_{TOT}} \left| \frac{R}{T} \frac{dT}{dr} \right|$, where χ is the effective heat diffusivity and the approximation corresponds to assuming $T_i=T_e$. Q_{NBI} is the heat flux from neutral beams and Q_{TOT} is the total heat flux. Γ/Q_{NBI} is determined by the beam energy spectrum. χ/D can be treated as a free parameter, whilst all the other terms in Γ^* can be evaluated from parameters in the database.

2.2 Definition of the Regression Variables

A meaningful combination of data from different devices requires consistent definitions and measurements of the variables, especially of the regressed variable. Data with systematic errors in opposite direction from different devices are a major concern, because regressions tend to associate these with differences in the dimensionless operating domains of the devices, essentially ν_{eff}, $\rho^*$and Γ^*, thereby leading to erroneous extrapolations.

To overcome this problem, we have devised a method to obtain values of density peaking for JET AUG and JET derived with exactly the same procedure [Angioni NFlett 2006]. We have observed that density profile measurements from Thomson scattering and interferometry agree better in JET than in AUG. We therefore computed the line integrals along the chords of the AUG interferometer of all the JET profiles of the database, remapped onto a chosen AUG equilibrium. Using the same equilibrium, we inverted the line integrals of the JET profiles by expressing the profiles as linear combinations of base functions for the profile shape. Finally, by the same method we also inverted all the AUG density profiles. In this way a set of density profiles, for both AUG and JET, reconstructed from the AUG interferometer line integrals by the same inversion method is obtained. Among the various possible definitions of density peaking, the definition of density peaking $n_e(\rho_{pol} = 0.2)/\langle n_e \rangle_{vol}$ is rather independent of the choice of the basis functions for the inversion, and strongly constrained, once all the line integrals are matched. The RMSE between the original JET density peaking [Weisen 2006], calculated using the SVDI method [Furno] with basis functions adjusted from shot to shot and the recalculated peaking with fixed basis functions is only 0.018.

2.3 Bivariate Correlations

Fig. 1 shows a selection of correlation plots. The related correlation coefficients are quoted in the figure, in black for the combined database, in red for AUG data only and in blue for JET data only. Those in smaller fonts indicate the correlation coefficients for the subset of plasmas heated

by NBI only. The combined database is composed of 277 JET observations and 343 AUG observations. Correlations with ρ* are strongly reduced by combining the two devices, but the correlation with the Greenwald fraction N_{GR} remains rather large. Collisionality is the parameter which has the largest correlation with density peaking in the combined dataset. However both the Greenwald fraction and the beam particle source parameter Γ* are also highly correlated with density peaking. Finally, a very strong correlation between ν_{eff} and Γ* in AUG plasmas heated with NBI only is found. This correlation is reduced by considering data from the two devices and by including data from ICRH-only discharges.

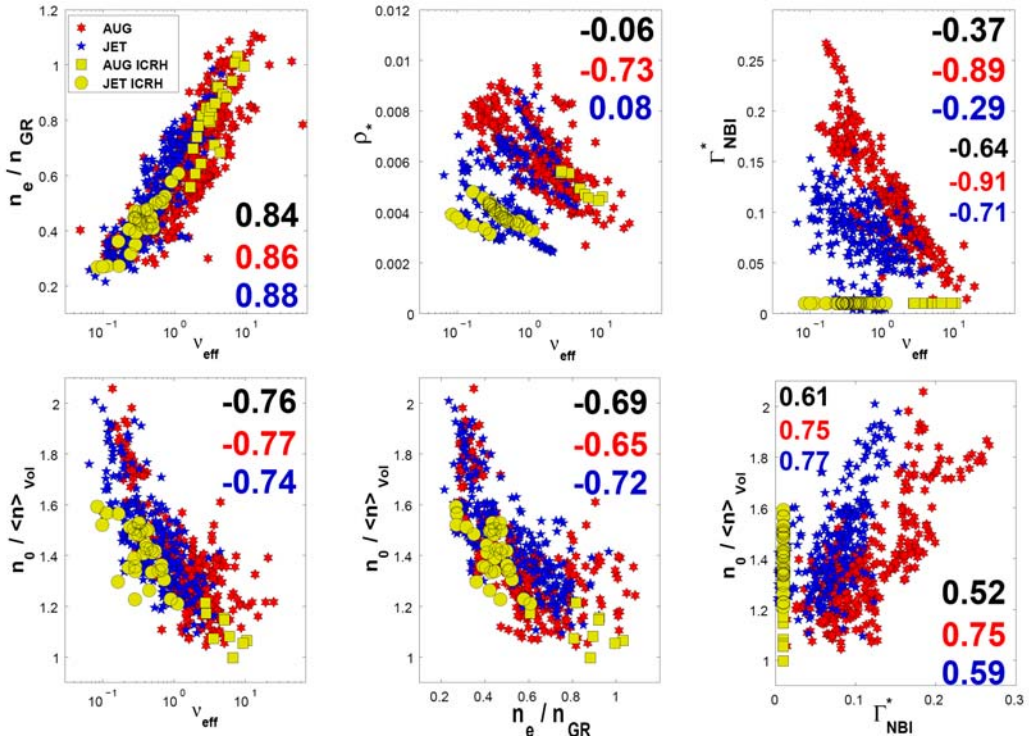

Fig.1 Selection of scatterplots with correlation coefficients (in small for NBI only).

2.4 Multivariate Statistical Analysis

Linear and logarithmic multivariable regressions express the regressed variable Y in the forms $Y=a_0+\sum_j a_j X_j$ and $Y=a_0\prod_j X_j^{a_j}$, where X_j are the regression variables and a_j the regression coefficients. Linear and logarithmic regressions having provided equivalent results in this study, due to the modest variation of the regressed variable $n_e(0.2)/\langle n_e\rangle_{vol}$, we'll only consider the former here. Following [Kardaun], we define the normalised statistical relevance StR_j and significance StS_j of the regression variable X_j as: $StR_j=a_j\times STD(X_j)/STD(Y)$ and $StS_j=a_j/STD(a_j)$, where STD designates the usual standard deviation.

Table 1 shows the normalised statistical relevance obtained for regressions involving different variables. The statistical significance is seen in table 2 for the same set of regressions. For a parameter X_j to be significant, $|StS_j|>2$ is required. Regressions which include ν_{eff} and exclude N_{GR}, which include N_{GR} and exclude ν_{eff}, as well as regressions which include both these plasma parameters, are considered. Moreover, for comparison, models which, besides the dimensionless variables, also include a device label (namely R_0) are analysed. In all the regression models which include it, ν_{eff} is found to be the parameter with the largest statistical relevance and has a large statistical significance.

TABLE 1: NORMALISED STATISTICAL RELEVANCE OF MAIN VARIABLES AND RMSE FOR DIFFERENT REGRESSION MODELS

Variables excluded	Γ^*	$\ln\nu_{eff}$	N_{GR}	ρ^*	β	q_{95}	δ	$T_{e2}/\langle T_e\rangle$	R_0	rmse
N_{GR}	0.39	-0.49		0.13	-0.24	-0.07	-0.08	0.03	0.25	0.113
N_{GR} & R_0	0.34	-0.64		-0.02	-0.16	-0.1	-0.014	-0.007		0.114
$\ln\nu_{eff}$	0.49		-0.30	0.14	-0.17	0.01	-0.08	-0.028	0.47	0.121
$\ln\nu_{eff}$ & R_0	0.42		-0.61	-0.27	0.09	-0.001	0.114	-0.12		0.126
None	0.39	-0.57	0.13	0.20	-0.31	-0.08	-0.12	0.036	0.29	0.112
R_0	0.34	-0.68	0.05	-0.005	-0.18	-0.10	-0.027	-0.008		0.114

TABLE 2: STATISTICAL SIGNIFICANCE OF MAIN VARIABLES FOR ABOVE REGRESSION MODELS

Variables excluded	Γ^*	$\ln\nu_{eff}$	N_{GR}	ρ^*	β	q_{95}	δ	$T_{e2}/\langle T_e\rangle$	R_0	rmse
N_{GR}	5.2	-5.24		1.0	-2.5	-1.1	-1.2	0.5	2	0.113
N_{GR} & R_0	4.8	-10.2		-0.2	-1.7	-1.5	-0.2	-0.1		0.114
$\ln\nu_{eff}$	7.3		-3.0	0.9	-1.5	0.2	-1.1	-0.4	4.1	0.121
$\ln\nu_{eff}$ & R_0	6.2		-8.5	-2.5	0. 9	-0. 1	1.8	-2		0.126
None	5.2	-4.3	0.9	1.4	-2.6	-1.2	-1.5	0.6	2.2	0.112
R_0	4.7	-5.3	0.4	-0.04	-1.7	-1.6	-0.4	-0.1		0.114

Comparable RMSE is found when the device label is included or excluded. In regression models which include ν_{eff} and exclude R_0, ρ^* is found to have a negligible statistical significance and relevance. In regression models which include N_{GR} and exclude ν_{eff}, R_0 plays a more important role, through a larger statistical relevance of ρ^* and/or R_0. At the same N_{GR}, the density peaking is larger in JET than in AUG. In regression models which exclude ν_{eff} and include N_{GR}, Γ^* is found to have a larger statistical relevance. Finally, in regression models which include both ν_{eff} and N_{GR}, density peaking increases with increasing N_{GR} at fixed ν_{eff} .The significance of ν_{eff} is not only larger than that of all other variables considered separately, but also larger than that of the pair (N_{GR}, R_0) and comparable to the pair (Γ^*, N_{GR}) [Angioni NF lett]. The pair (ν_{eff} , Γ^*) has the highest significance of all pairs.

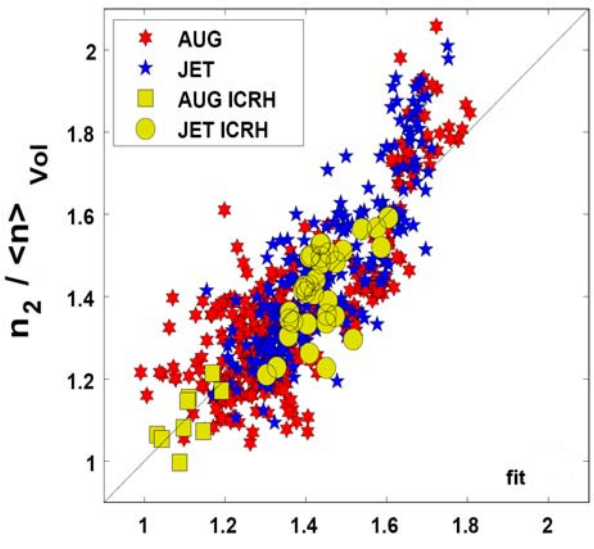

An example of a scaling relation (fig.2) without N_{GR} is given as

$n_{e2}/\langle n_e\rangle = 1.35\pm0.015 - (0.12\pm0.01)\ln\nu_{eff} + (1.17\pm0.01)\Gamma^* - (4.3\pm0.8)\beta$

Extrapolation to ITER predicts a density peaking given by $n_e(0.2)/\langle n_e\rangle\approx1.45$. For ITER we assumed $\langle T_e\rangle$ = 8 keV and $\langle n_e\rangle = 10^{20}m^{-3}$, N_{GR}=0.85 and Γ^*=0. All regressions using ν_{eff} as one of the regression variables predict $n_e(0.2)/\langle n_e\rangle>1.35$ for ITER, whilst nearly all those excluding ν_{eff} predict $n_e(0.2)/\langle n_e\rangle<1.2$.

Fig.2 Experimental versus fitted density peaking

3) Influence of Specific Parameters and Comparison with theory

The collisionality dependence of the anomalous pinch predicted by gyrofluid drift wave turbulence models [Weiland, Angioni 2003] is qualitatively consistent with the above observations in H-mode. However the collisionality dependence in gyrokinetic models is still an issue under investigation [Angioni, Estrada-Mila].

The combined AUG-JET database does not have T_i and q profiles. Regressions involving these quantities have been performed on a subset of the JET database [Weisen 2006]. They are consistent with the results from the combined database and confirm a lack of a dependence on local magnetic shear, global shear (l_i) and on the normalised temperature gradients. These observations are at odds with theoretical expectations for the curvature pinch and thermodiffusion [Garbet]. However JET data reveal a modest dependence on the theoretically important temperature ratio T_i/T_e, expressed in the scaling relation obtained from a subset of 114 JET samples:

$$n_{e2}/\langle n_e\rangle = 1.15\pm0.07 - 0.12(\pm0.02)\ln\nu_{eff} + 0.17(\pm0.13)D\Gamma^*/\chi + 0.13(\pm0.08)T_i/T_e$$

In the above expression T_i/T_e and $D\Gamma^*/\chi$ are taken at mid-radius (Calculating $D\Gamma^*/\chi$ does not require D, see definition in section 2). An extrapolation to ITER, using this fit and assuming $T_i/T_e=0.9$, provides $n_{e2}/\langle n_e\rangle\approx1.47$, consistently with the combined database. A local fit to the normalized density gradients around mid-radius provides

$$R\nabla n_e/n_e = 0.97\pm0.34 - (0.65\pm0.1)\ln\nu_{eff} + (1.46\pm0.63)D\Gamma^*/\chi + (0.65\pm0.4)T_i/T_e$$

The coefficient of the local fit for $D\Gamma^*/\chi$ is an estimate for χ/D and is consistent with theoretical expectations [Garbet]. The scaling relations leads to an expectation of $R\nabla n_e/n_e\approx2.6$ near mid-radius in ITER.

The observation that density profiles tend to be flatter at low values of T_i/T_e is in qualitative agreement with theory. A concern for a reactor is that the large core electron heating by slowing-down alpha particles may destabilise TEMs. TEMs drive a thermodiffusive outward particle flux, which may lead to partial or complete flattening of the density profile [Garbet, Angioni]. This cannot be tested at JET yet, because purely ICRH heated H-modes in JET only have $\beta_N\sim1$, due to a lack of available power. However purely electron heated H-modes with $\beta_N\cong2$ and $T_e/T_i\cong2$, recently obtained in TCV using ECH, show that flattening is only partial and significantly peaked density profiles ($n_{e2}/\langle n_e\rangle\sim1.5$ in TCV ELMy H-modes) persist in electron heated regimes at reactor relevant values of β_N, even when T_e is significantly above T_i (fig.3). The weakness of the T_e/T_i dependence in JET and the observations in TCV suggest that flattening of the density profile in ITER as a result of α-heating is unlikely.

As for JET, peaking in these TCV plasmas cannot be explained by the Ware pinch, unless very low values of D/χ are assumed. To maintain the observed density gradients, $\nabla n_e/n_e\sim5m^{-1}$, with typical $V_{ware}\sim0.3$m/s, D would have to be about $0.06m^2/s$ i.e. 50 times smaller than χ. The neutral source from the edge, simulated with Kn1D and DOUBLE codes [Zab2006] is, as in JET, too shallow to explain the peakedness of the density profiles in a purely diffusive model, unless the ratio D/χ is assumed to vary by more than two orders of magnitude within the confinement zone of the plasma (fig. 4).

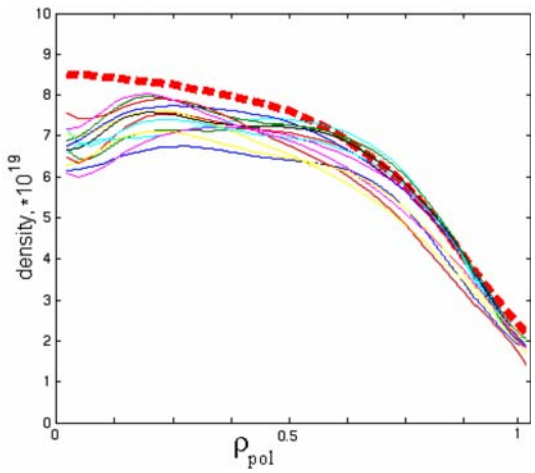

Fig.3 : Multiple TS measurements of density profiles during ECH heating in ELMy H-mode in TCV. Red dashed line – density profile in an Ohmic H-mode plasma.

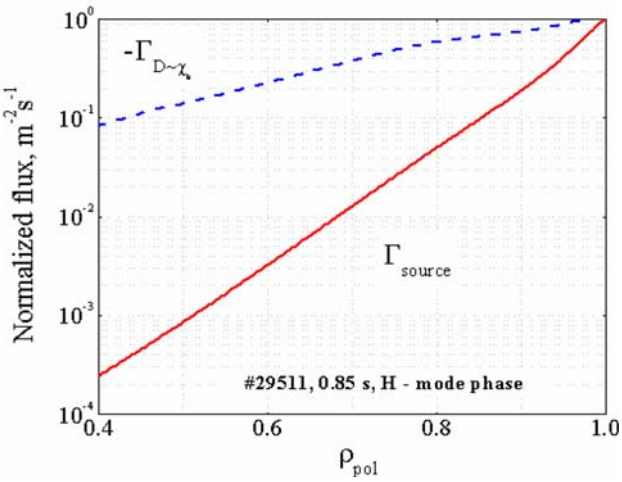

Fig.4: Kn1D simulation of edge neutrals flux and comparison with particle diffusive flux, assuming $D \propto \chi$, for ECH heated H-mode plasma on TCV.

4) Impact on Reactor Fusion Performance

We have treated each of the n_e, T_e profile pairs in the JET database as a potential model for ITER by renormalizing the density and the temperature to the ITER parameters for the inductive scenario, i.e. $\langle n_e \rangle = 1.01 \times 10^{20} m^{-3}$ and $\beta_N = 1.8$ and the plasma volume to $831 m^3$. We assumed $T_i = T_e$ and the dilution was adjusted such as to obtain a thermonuclear fusion power $P_{fus} \equiv 17.6 \times 10^6 \int \langle \sigma v \rangle n_D n_T dV = 400 MW$ (corresponding to Q=10) for a flat density profile and an ITER-like temperature profile as in ref [Mukh], with $T(0.95)/T(0) \cong 0.18$ and $T(0) \cong 22 keV$. Fig.5 shows the resulting fusion power, resolved into classes of relative pedestal temperature, T(0.95)/T(0). In addition to the dependence on density peaking, there also is a strong dependence on T(0.95)/T(0), large temperature pedestals being unfavourable for fusion performance when operation is restricted to a fixed value of stored energy, corresponding to the restriction of a particular operating scenario (This only reverses for T(0)>40keV). Note that most temperature profiles in JET are broader than those in [Mukh].

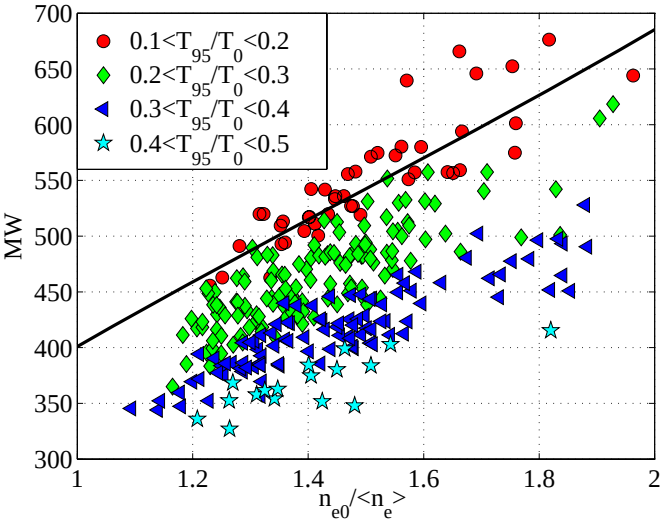

Fig 5: Fusion power versus density peaking, resolved into classes of relative edge temperature, assuming $\langle n_e \rangle = 1.01 \times 10^{20} m^{-3}$, $\beta_N = 1.8$ and $V = 831 m^3$ with density and temperature profile shapes from JET database. The line is for a temperature profile similar to ITER simulations in ref [Mukh]. The symbols refer to different classes of relative temperature pedestals.

For peaking exceeding the above ITER predictions, the alpha power increase may in principle substitute for the auxiliary power (40 MW), allowing ignition (assuming confinement and dilution are unaffected by profile shapes). Only a small number of the n_e,T_e profile pairs in the

JET database (those with P_{fus}>600MW in fig.5) are however peaked enough and all of those have significant beam fuelling. Beam fuelling will be insignificant in ITER.
The fusion power in these ITER models for fixed β and $\langle n_e \rangle$ scales very closely to $\langle p^2 \rangle / \langle p \rangle^2$, as expected from the nearly quadratic dependence of $\langle \sigma v \rangle$ on T_i in the region 7-20keV, which corresponds to most of the plasma volume in the ITER inductive and hybrid scenarios. We may therefore use $\langle p^2 \rangle / \langle p \rangle^2$ as a figure of merit for the pressure profile. Fig. 6 shows that fusion performance increases in a very similar fashion as density peaking when the collisionality decreases.

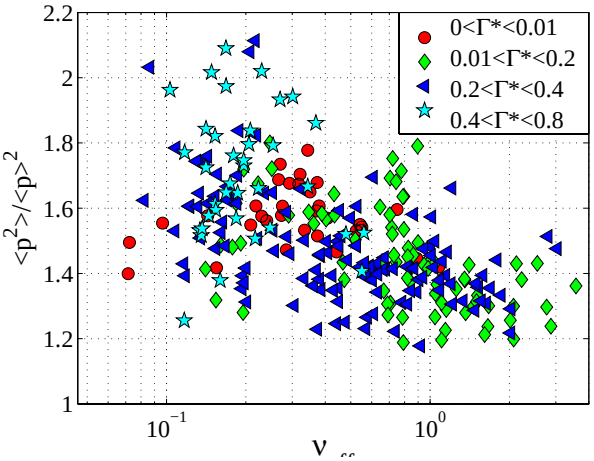

Fig 6. Pressure profile figure of merit versus collisionality in JET. Symbols refer to classes of dimensionless beam source.

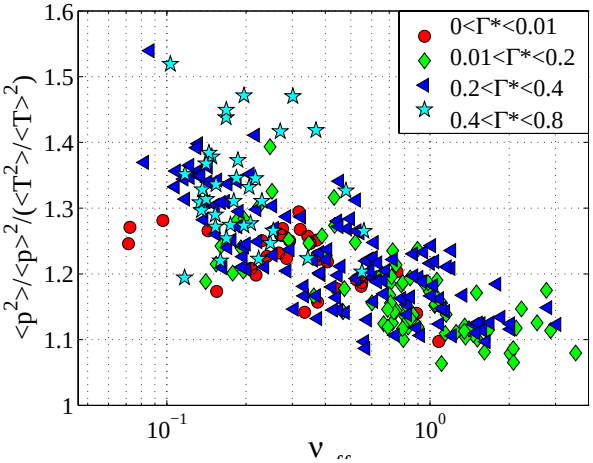

Fig 7. Density contribution to the pressure profile figure of merit.

On the other hand $\langle T^2 \rangle / \langle T \rangle^2$ shows no significant correlation with any of the dimensionless parameters, thereby demonstrating that the beneficial effect of density peaking and is not cancelled by temperature profile broadening, as 'pressure profile consistency' theories might suggest. For typical JET profiles at low collisionality, the fusion performance improvement attributable to density peaking, quantitatively expressed by the ratio $\langle p^2 \rangle \langle T \rangle^2 / (\langle p \rangle^2 \langle T^2 \rangle)$, amounts to some 30%, as seen in fig 8. Instead of regressing the density peaking factor, we may also regress the above profile merit factors. These lead to $\langle p^2 \rangle / \langle p \rangle^2 \approx 1.55$ and $\langle p^2 \rangle \langle T \rangle^2 / (\langle p \rangle^2 \langle T^2 \rangle) \approx 1.25$ expected for ITER by regressions including collisionality as a regression variable.

A drawback of density peaking is an increased proneness to heavy impurity accumulation. Whereas carbon density profiles from CXS remain close to flat irrespectively of collisionality in JET H-modes [weisen 2005], core accumulation of laser ablated Ni has been observed in some JET discharges at $\nu_{eff} \sim 0.1$[Puiatti]. Accumulation of tungsten in AUG has been shown to be preventable with central electron heating [Dux?]. On the downside we also have to consider that for fixed N_G and β, density peaking unavoidably leads to a reduction of the pedestal density below the average density, by some 25% for the above ITER projections [Weisen 2006]. This may affect divertor performance by making detachment more difficult. If however the density limit is linked to the pedestal density, rather than to the line average density, a simple remedy is to raise the edge density to the target value with a corresponding temperature reduction to conserve β. In this case the effect of peaking is still beneficial, although somewhat less than at fixed average density [Weisen 2006]. Density peaking may also provide a natural means to salvage core fusion performance (but not divertor performance) if the edge density limit drops to half of the expected value [Borrass].

Conclusions

Studies on JET, AUG and TCV have clearly established the anomalous nature of density peaking in H-mode, i.e. this phenomenon cannot be explained by the Ware pinch, nor the particle source, although the latter is a contributor in beam heated discharges. The most important parameters for peaking are collisionality, the beam source (where applicable) and the Greenwald fraction. Scaling expressions including collisionality predict fairly peaked density profiles for ITER, providing a fusion power increase of up to 30%, while scalings excluding it predict fairly flat profiles for ITER. Although clearly anomalous, many observations of density profile behaviour are still challenges for physics based theoretical modelling. These include the apparent lack of correlation of density peaking with magnetic shear in H-mode (albeit observed in L-mode, [Zab2003, Weisen 2004] and with temperature peaking and the abrupt collisionality dependence of pinches in gyrokinetic models. The relatively broad scatter of the regression fits, which exceeds experimental errors, also suggests the existence of factors influencing density peaking, which have yet to be experimentally identified.

Acknowledgement: This work was partly supported by the Swiss National Fund for Scientific Research.

References

[1] G.T. HOANG et al, Phys. Rev. Lett. **90** (2003) 155002
[2] A. ZABOLOTSKY et al, Plasma Phys. Contr. Fusion **45** (2003) 735
[3] H. WEISEN et al, Plasma Phys. Controll. Fusion **46** (2004) 751
[4] A. ZABOLOTSKY et al, Nucl. Fusion **46** (2006) 594
[5] H. WEISEN et al, Nuclear Fusion **45** (2005) L1-L4
[6] H. WEISEN et al, Plasma Phys. Control. Fusion **48** (2006) A457
[7] D.R. BAKER et al, Nucl. Fusion **40** (2000) 1003
[8] H. WEISEN & E. MINARDI, Europhysics Letters **56** (2001) 542
[9] C. ANGIONI et al, Phys. Rev. Lett. **90** (2003) 205003
[10] C. ANGIONI et al, Phys. Plasmas **12** (2005) 112310
[11] C. ESTRADA-MILA et al, Phys. Plasmas **12** (2005) 022305.
C. ESTRADA-MILA, J. CANDY, AND R. E. WALTZ Phys. Plasmas **13** (2006) 074505
[12] C. ANGIONI et al, submitted to Nucl. Fusion
[13] I. FURNO et al, Plasma Phys. Control. Fusion **47** (2005) 49
[14] O.J.W.F. Kardaun, Classical Methods of Statistics, Springer Verlag 2005.
[15] J. WEILAND et al, Nucl. Fusion **29** (1989) 1810
[16] X. GARBET et al, Plasma Phys. Controll. Fusion **46** (2004) B577
[17] V. MUKHOVATOV et al, Nucl. Fusion **43** (2003) 942–94
A.R. POLEVOI et al, J. Plasma Fusion Res. Series **5** (2002) 82
[18] M.E. PUIATTI et al, Phys. Plasmas **13**, 042501 (2006)
[19] DUX, need reference
[20] K. BORRASS et al., Nuclear Fusion **44** (2004) 752